

# Reasoning mechanism: An effective data reduction algorithm for on-line point cloud selective sampling of sculptured surfaces<sup>☆,☆☆</sup>



Yan Li <sup>a</sup>, Haibo Liu <sup>b</sup>, Ye Tao <sup>a,c,\*</sup>, Jianxing Liao <sup>c</sup>

<sup>a</sup> School of Manufacturing Science and Engineering, Sichuan University, Chengdu 610065, China

<sup>b</sup> School of Mechanical Engineering, Dalian University of Technology, Dalian 116024, China

<sup>c</sup> Energy Research Center of Lower Saxony (EFZN), Goslar 38640, Germany

## ARTICLE INFO

### Article history:

Received 13 August 2018

Received in revised form 21 January 2019

Accepted 5 April 2019

### Keywords:

Sculptured surface  
Reasoning mechanism  
Data reduction  
Point cloud  
Selective sampling

## ABSTRACT

For obtaining a high-quality profile of measured sculptured surface, scanning devices have to produce massive point cloud data with great sampling rates. Bottlenecks are created owing to inefficiencies in storing, manipulating and transferring these data, and the parametric modeling from them is quite a time-consuming work. The purpose of this paper is to effectively simplify point cloud data from a measured sculptured surface during the on-line point cloud data selective sampling process. The key contribution is the generation of a novel reasoning mechanism which is based on a predictor-corrector scheme, and it is capable of eliminating data redundancy caused by spatial similarity of collected point clouds. In particular, this mechanism is embedded in our newly designed framework for on-line point cloud data selective sampling of sculptured surfaces. This framework consists of two stages: First, the initial point data flow is selective sampled using bi-Akima method; second, the data flow is refined based on our proposed reasoning mechanism. Moreover, our versatile framework is capable of obtaining high-quality resampling results with smaller data reduction ratio than other existing on-line point cloud data reduction/selective sampling methods. Experiment is conducted and the results demonstrate the superior performance of the proposed method.

© 2019 Elsevier Ltd. All rights reserved.

## 1. Introduction

Sculptured surface parts are being utilized more and more widely in modern industries. These involve, but are not limited to, aerospace, aviation, shipbuilding, automotive, biomedical and home appliance industries. The manufacture of a sculptured surface part often begins with the description of its function and produces a geometric computer aided design (CAD) model suitable for manufacturing effectively in forward engineering [1]. However, CAD models are not always available in the production environment in many cases. Reverse engineering makes it feasible to create a CAD model of a part that has no design data or has gone through many design changes, which can significantly improve product design quality. This technology enables us to recreate an existing part by reconstructing its surface geometry

in 3D digital files using point cloud data which is obtained from the scanning measuring devices [2–5].

Nevertheless, these scanning devices produce extremely dense point data at great sampling rates [6], and not all these point data are necessary for generating a CAD model [7–9]. Moreover, bottlenecks are created owing to inefficiencies in storing, manipulating and transferring them. The acquired data require a large storage space and the generation of parametric model from them is rather a time-consuming work [10]. Reducing the amount of scanned data while maintaining the required accuracy is a crucial task for point cloud data preprocessing [11]. Under the premise of ensuring the accuracy, describing an object with the least point cloud information is always an expectation [12,13]. Thus, a high-quality point cloud data reduction/selective sampling method for sculptured surface is being pursued all the time [14].

### 1.1. Related work

Until now, the most representative data sampling methods for sculptured surface scanning measurement typically include isochronous sampling and equidistant sampling [15]. Both are easy to implement, but neither can adjust the point cloud density according to the required accuracy and surface curvature adaptively. They cannot minimize the amount of point cloud data

☆ This paper has been recommended for acceptance by H. S. Shin.

☆☆ No author associated with this paper has disclosed any potential or pertinent conflicts which may be perceived to have impending conflict with this work. For full disclosure statements refer to <https://doi.org/10.1016/j.cad.2019.04.002>.

\* Correspondence to: School of Manufacturing Science and Engineering, Sichuan University, No.24 South Section 1, Yihuan Road, Chengdu 610065, China.

E-mail address: [yetao@scu.edu.cn](mailto:yetao@scu.edu.cn) (Y. Tao).

while guaranteeing the sampling accuracy [16]. To address these issues, a multitude of data reduction/simplification algorithms for massive point cloud scanned from sculptured surface were developed, which can be divided into two categories:

### 1.1.1. Off-line point cloud data reduction/simplification

Song and Feng [10] showed a point cloud simplification algorithm to reduce the number of data points scanned from a mechanical part in which the boundary surfaces often contain sharp edges. This algorithm identifies edge points first and then progressively removes the least important data point until the specified data reduction ratio is reached. Chen et al. [1] proposed a data reduction method based on bi-directional point cloud slicing strategy, point cloud can be reduced while considering geometric features. Shi, Liang and Liu [7] presented a new adaptive simplification method to reduce the number of the scanned dense points. An automatic recursive subdivision scheme is designed to pick out representative points and remove redundant points. Ma and Cripps [17] gave a new point cloud data reduction algorithm to preserve the original shape using an error metric based on a Hausdorff distance of principal curvature vectors. Smith, Petrova, and Schaefer [18] presented a new method for compressing surfaces created from oriented points. This method uses octree algorithm to remove redundant data, and the oriented points are sampled using a laser range scanner or created from polygonal surfaces. Morell et al. [19] propose a 3D lossy compression system based on plane extraction which represent the points of each scene plane as a Delaunay triangulation and a set of points/area information. Khameneifar and Feng [8] presented a method to extract cross-sectional contour profiles of a physical object from the massive point cloud, which contains a lot of redundant data. The extracted data point is approximated by fitting a local quadric surface to the neighboring points of the point of interest. Chen et al. [20] propose a point cloud resampling method based on centroidal Voronoi tessellation (CVT). The CVT on a point cloud is efficiently computed by restricting the Voronoi cells to the underlying surface, which is locally approximated by a set of best-fitting planes.

These attempts have been focused on achieving the best data reduction effect based on manipulating polyhedral models or iterative solutions. However, these methods pay more attention to the qualitative description of surface features rather than the quantitative retention of accuracy features. That is, the accuracy of reduced data cannot be controlled under a certain required accuracy. Moreover, it is impossible to achieve on-line data reduction during the real-time sculptured measuring process when using these methods, for they can only reduce the whole point cloud data during the off-line data post processing. Data sampling and data reduction processes are completely separated, and massive storage space is occupied by a huge amount of point cloud data in data acquisition equipment. The processing and transmission of surface information takes up a significant amount of time and hardware resources, which will undoubtedly affect the efficiency of surface model reconstruction and product redesign.

### 1.1.2. On-line point cloud data reduction/selective sampling

Above issue has captured the attention of researchers all over the world, and some on-line point cloud data reduction/compression methods have been proposed. Herein, data sampling process and on-line data reduction process are carried out simultaneously, thus they make up the selective sampling process.

ElKott and Veldhuis [21] presented a selective sampling approach of sculptured surfaces based on scanning isoparametric lines. The locations of the sample lines are extracted from the

surface CAD model based on the change in surface curvature, and these lines are fitted to construct a substitute geometry of the surface. The accuracy of the sampling plan is characterized by the maximum deviation between the substitute geometry and the surface CAD model. Although the algorithm presented in this work enables selective sampling of sculptured surfaces, it still has the following limitations: (i) The algorithm can only operate on sculptured surfaces with original CAD models. Moreover, it is restricted to CAD models with only one NURBS surface. (ii) Trimmed surfaces, spliced surfaces and surfaces with multiple/sharp edges cannot be sampled using the presented algorithms. The above limitations reduce the practicability of the algorithm, and narrow the scope of its application.

Wozniak, Balazinski, and Mayer [22] proposed a method of measured point determination for selective sampling with the application of fuzzy logic in coordinate metrology. It works on a series of selected points obtained by contact scanning of the measured surface. The outline of the current scanning path defines an arc for each measured point, each such arc being delimited by the points of intersection with the preceding and the following arcs. According to the arc of each measured points, a rule-based approach to decision making using fuzzy logic techniques is proposed for point determination. Jia et al. [23] proposed a new point cloud data accept and reject method in order to enhance the sampling precision and efficiency in free-form surface scan-tracking measurement. This method combines isochronous indistinctive sampling with equal-error accurate arithmetic. It has the ability of accept and reject the sampling data reasonably based on the curvature changes, and it can achieve higher measurement accuracy with less sampling data. The essence of the above two on-line data selective sampling methods [22,23] is the same, both of which are based on equal arc-to-chord deviation reduction (EACDR) method. Herein, the deviation is quantified by the maximum distance between the arc formed by the original dense point set and the chord formed by the extracted two adjacent sample points. The EACDR method can reduce the dense point data during the real-time data sampling process under a certain tolerance. Its algorithm is very simple and it is ideal for on-line data reduction. Unfortunately, the EACDR method specifies that all discrete dense point sets must be connected by straight segments. Hence, the reconstructed surface of the CAD model is certainly not smooth and there are many cusp points [24], which undoubtedly affects the quality of surface reconstruction.

In view of this limitation, Tao et al. [16] proposed an on-line point cloud data extraction algorithm for spatial scanning measurement of sculptured surface. In this work, bi-Akima method was presented for smoothly connecting spatial point sequence. Under the effect of bi-Akima method, the data extraction algorithm can obtain a smaller data reduction ratio and a smoother reconstructed surface than previous method under the same required accuracy during the real-time scanning measuring process. Furthermore, it can handle point sets of arbitrary and varying size, point density, and scanning line shape. The above advantages prove that the bi-Akima method is more suitable for on-line point cloud data reduction/selective sampling than previous work. However, this method can only extract points from the dense point set on a single scan line that are currently being measured, and cannot eliminate data redundancy between all point sets of the measured portion of the surface. There is still room for further improvement.

## 1.2. Our intention

Existing on-line point cloud data reduction/selective sampling methods mentioned above can only eliminate data redundancy based on the point set of the current scanning line. Nevertheless,

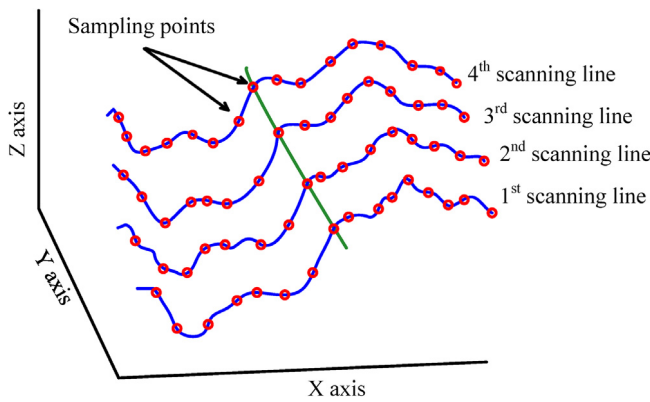


**Fig. 1.** Schematic of point cloud data spatial arrangement.

most of sculptured surface scanning devices adopt layer-by-layer scanning path (e.g., contact 3D scanning probes, CCD laser triangle displacement sensors, 3D-laser scanners, industrial CT systems, etc.), adjacent scanning lines are extremely similar in shape. Take Fig. 1 as an example, there are four scanning lines of a certain measured surface. Obviously, the shape of the scanning lines and the spatial distribution of the sampling points are actually quite similar. The geometric feature similarity between such layers is bound to result in data redundancy, which makes it possible to further compress the sampled point data.

This paper focus on how to effectively simplify point cloud data from a measured sculptured surface during the on-line data selective sampling process, while ensuring that data accuracy does not deteriorate. Our core contribution is the generation of a novel reasoning mechanism for on-line point cloud data selective sampling, which is based on a predictor–corrector scheme. It can estimate the point set spatial arrangement of the current scanning line based on the characteristics of previously scanned lines during the data sampling process. Therefore, data redundancy caused by the similarity between adjacent scanning lines can be eliminated. Furthermore, a new framework which contains the reasoning mechanism is designed for on-line point cloud data selective sampling of sculptured surface, and it is capable of obtaining high-quality resampling results with smaller data reduction ratio than other existing on-line point cloud data reduction/selective sampling methods. *To the best of our knowledge, this is the first study to solve the problem of data redundancy caused by the geometric feature similarity between scan layers during the on-line point cloud data sampling of sculptured surface.*

The rest of this paper is organized as follows: In Section 2, the principle of the proposed framework for on-line point cloud data selective sampling, and the algorithm of the reasoning mechanism is described in detail. The validations of the proposed algorithm with the scanned point clouds are given in Section 3. Finally, some conclusions are drawn from this paper in Section 4.

## 2. Approach description

The proposed framework for on-line point cloud data selective sampling of sculptured surface generally consists of two stages as shown in Fig. 2. The initial point cloud data flow is obtained by conventional isochronous sampling or equidistant sampling method, and then the first stage of our approach is to perform selective sampling by bi-Akima method, which is able to reduce the initial point cloud data flow of the current scanning layer. Afterwards, the second stage makes data resampling using reasoning mechanism according to the reduced point cloud data flow which is obtained from the first stage. Finally, the refined data flow is transmitted to the storage space of the measurement system. The detailed process for each stage is described in Sections 2.1 and 2.2 below.

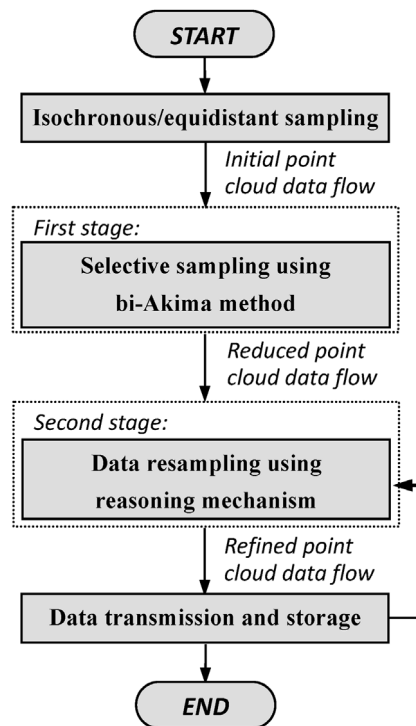


**Fig. 2.** The framework for on-line point cloud data selective sampling of sculptured surface.

### 2.1. First stage: selective sampling of current single scanning layer

In this stage, the initial point cloud data flow is first selectively sampled by bi-Akima method. It builds a bi-Akima curve interpolation algorithm for on-line reduction of point cloud data flow. It receives initial point cloud data flow from the scanning devices and outputs reduced point cloud data flow immediately. This paper only gives a brief description of this method and the details of which are described in our previous work [16].

#### 2.1.1. Brief description of bi-Akima interpolation

Bi-Akima curve is relying on a pair of piecewise functions, each of which is composed of a set of cubic polynomials. The coefficients of each polynomial between a pair of given points are determined by the coordinates of and the slopes at these two points. At each given point, the slopes are determined by the coordinates of five points: a center point and two points on each side of it. The slopes  $t_{y,i}$ ,  $t_{z,i}$  of the curve at point  $P_i(X_i, Y_i, Z_i)$  are determined by

$$\begin{cases} t_{y,i} = \frac{|m_{y,i+1}-m_{y,i}|m_{y,i-1} + |m_{y,i-1}-m_{y,i-2}|m_{y,i}}{|m_{y,i+1}-m_{y,i}| - |m_{y,i-1}-m_{y,i-2}|}, \\ t_{z,i} = \frac{|m_{z,i+1}-m_{z,i}|m_{z,i-1} + |m_{z,i-1}-m_{z,i-2}|m_{z,i}}{|m_{z,i+1}-m_{z,i}| - |m_{z,i-1}-m_{z,i-2}|}, \end{cases} \quad (1)$$

in which  $m_{y,i}$  and  $m_{z,i}$  are the slopes of projections of line segment  $P_iP_{i+1}$  in XOY and XOZ plane respectively, where  $i = 1, 2, 3 \dots n$ . The slopes  $t_{y,i}$  and  $t_{z,i}$  depend on the slopes of four line segments ( $P_{i-2}P_{i-1}$ ,  $P_{i-1}P_i$ ,  $P_iP_{i+1}$  and  $P_{i+1}P_{i+2}$ ). It is worth noting that two more points have to be estimated from the given points based on the trend of the given points:

$$\begin{cases} m_{y,0} = 2m_{y,1} - m_{y,2} \\ m_{y,-1} = 2m_{y,0} - m_{y,1} \\ m_{y,n} = 2m_{y,n-1} - m_{y,n-2} \\ m_{y,n+1} = 2m_{y,n} - m_{y,n-1} \end{cases} \text{ and } \begin{cases} m_{z,0} = 2m_{z,1} - m_{z,2} \\ m_{z,-1} = 2m_{z,0} - m_{z,1} \\ m_{z,n} = 2m_{z,n-1} - m_{z,n-2} \\ m_{z,n+1} = 2m_{z,n} - m_{z,n-1} \end{cases}. \quad (2)$$

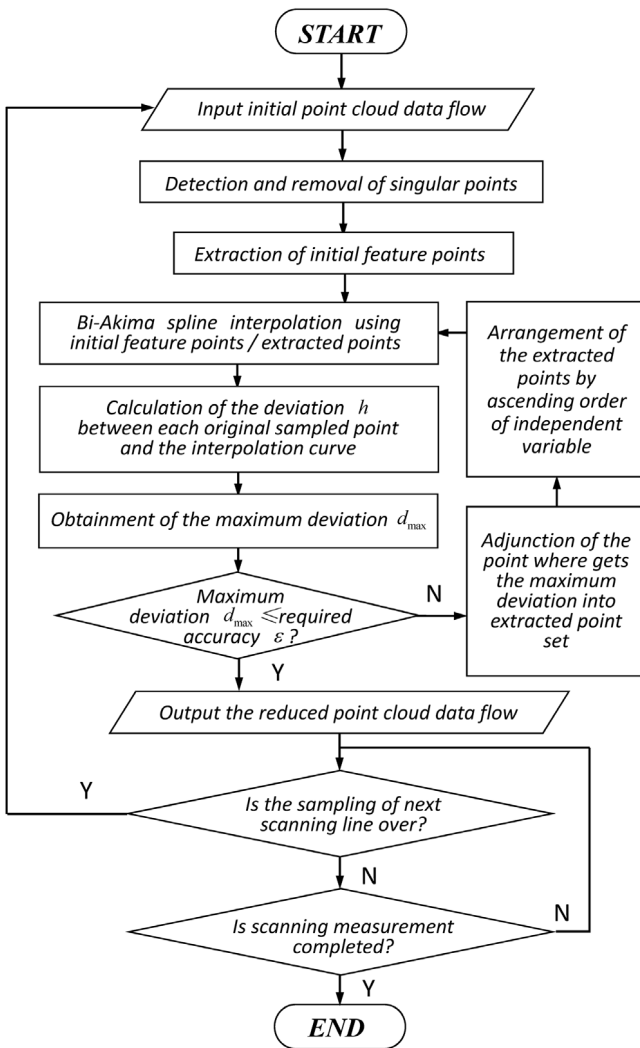


**Fig. 3.** The flow diagram of selective sampling process in the first stage.

In accordance with Eqs. (1) and (2), the polynomials can be determined uniquely. Thus, each pair of piecewise functions can be formulated as:

$$\begin{cases} y = A_y + B_y(x - X_i) + C_y(x - X_i)^2 + D_y(x - X_i)^3 \\ z = A_z + B_z(x - X_i) + C_z(x - X_i)^2 + D_z(x - X_i)^3 \end{cases} \quad (3)$$

in which

$$\begin{cases} A_y(i) = Y_i \\ B_y(i) = t_{y,i} \\ C_y(i) = \frac{3m_{y,i}-2t_{y,i}-t_{y,i+1}}{X_{i+1}-X_i} \\ D_y(i) = \frac{t_{y,i}+t_{y,i+1}-2m_{y,i}}{(X_{i+1}-X_i)^2} \end{cases} \text{ and } \begin{cases} A_z(i) = Z_i \\ B_z(i) = t_{z,i} \\ C_z(i) = \frac{3m_{z,i}-2t_{z,i}-t_{z,i+1}}{X_{i+1}-X_i} \\ D_z(i) = \frac{t_{z,i}+t_{z,i+1}-2m_{z,i}}{(X_{i+1}-X_i)^2} \end{cases} \quad (4)$$

Thus a complete curve is obtained, which is composed of several piecewise polynomials and passes through every chosen point without unnatural wiggles.

#### 2.1.2. Selective sampling process in the first stage

Based on bi-Akima curve interpolation algorithm, the flow diagram of the selective sampling process is shown in Fig. 3.

For purpose of depicting the broad contours of a curve using a certain sequence of points  $Q_j (j = 1, 2, 3, \dots, m)$ , initial feature

points should be extracted at first. We specify that the initial feature points include the following types:

(i) **The edge points.** For a certain scanning line, the edge points are the start point and end point, namely the first point  $Q_1$  and the last point  $Q_m$  of a certain point sequence. These two points must be extracted at first.

(ii) **The cusp points.** At these points, the curve has the local extrema of the curvature. These points reflect the maximum extent of the concave and convex so that they can describe the broad contour of a certain scanning line roughly. It is easy to find the cusp points for a continuous curve with analytical expression:

$$\kappa(s) = \lim_{\Delta s \rightarrow 0} \left| \frac{\Delta \theta}{\Delta s} \right|, \quad (5)$$

where  $\Delta \theta$  is the angle between tangent vectors  $\vec{\alpha}(s)$  and  $\vec{\alpha}(s+\Delta s)$  of two adjacent points,  $\Delta s$  is the arc length between these two points.

After initial feature points extraction, the initial feature points can be used as the extracted points  $P_i(X_i, Y_i, Z_i)$ . Then the extracted points are used for bi-Akima interpolation for the first time. After that, the curve is divided into several intervals by extracted points  $P_i$ . There is deviation  $h_j$  between each original sampled point  $Q_j$  and interpolated curve apart from the extracted points, where the deviation  $h_j$  means the shortest spatial distance  $s$  from every original sampled point  $Q_j$  to interpolated curve:

$$h_j = \min_{x \in (X_i, X_{i+1})} (s) = \min_{x \in (X_i, X_{i+1})} \left( \sqrt{(x - x_j)^2 + (y - y_j)^2 + (z - z_j)^2} \right), \quad (6)$$

where point  $Q_j(x_j, y_j, z_j)$  is an original sampled points between  $P_i(X_i, Y_i, Z_i)$  and  $P_{i+1}(X_{i+1}, Y_{i+1}, Z_{i+1})$ , and  $P_{curv}(x, y, z)$  is the point in interpolated curve that makes the distance  $s$  shortest.

The next step is to seek the maximum deviation  $h_{\max} = \max(h_j)$  in every interval between two extracted points  $P_i$  and  $P_{i+1}$ . Subsequently, compare the max deviation value  $h_{\max}$  of all intervals and obtain the max deviation of the whole curve  $d_{\max} = \max(h_{\max})$ . The max deviation  $d_{\max}$  is then compared with the required accuracy  $\epsilon$ . If  $d_{\max} > \epsilon$ , the point where gets  $d_{\max}$  will be added in the extracted points. Afterwards, repeat the process above till  $d_{\max} \leq \epsilon$  and output the reduced point cloud data flow.

#### 2.2. Second stage: re-sampling based on previous multi scanning layers

In this stage, the reasoning module receives reduced point cloud data flow from the first stage, and then further refines these data. This module generally includes several key aspects such as conjecture, search, speculation and verification. It is worth mentioning that the “reasoning mechanism” proposed and named in this paper is not a traditional artificial intelligence algorithm, but a mathematical method based on spline extrapolation to predict and correct sampling points. The flow chart of selective sampling using reasoning module is illustrated in Fig. 4. Sampled point cloud data can be further refined through the data processing of this module. That is, the amount of data becomes smaller. Its mechanism is described in detail as follows:

##### 2.2.1. Conjecture the curve shape and scanning direction of the current scanning line

Based on reduced point cloud data flow from the first stage, the reasoning mechanism first conjectures the curve shape and

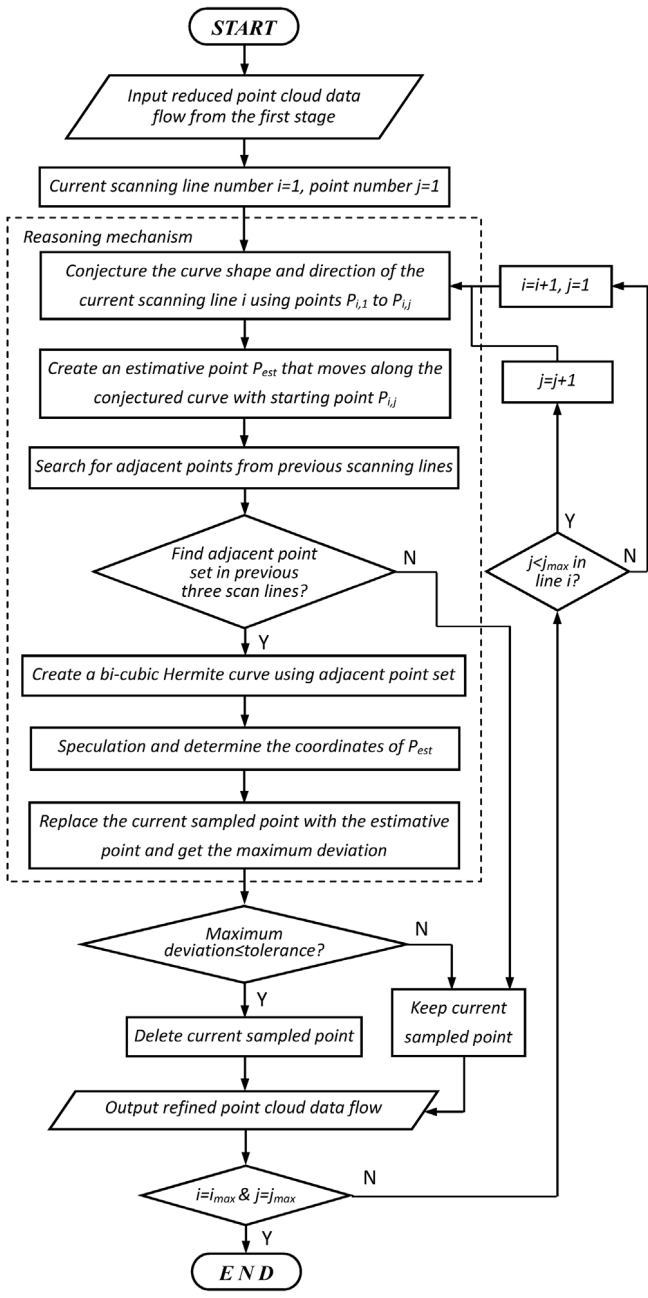


**Fig. 4.** The flow chart of selective sampling using reasoning mechanism.

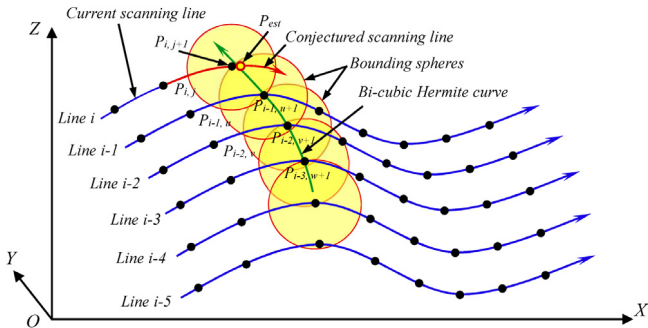


**Fig. 5.** The schematic diagram of reasoning mechanism.

scanning direction of the current scanning line. Herein, the conjecture is realized by the Hermite extrapolation. The algorithm is detailed as follows:

As shown in Fig. 5, line  $i$  is the current scanning line during the on-line measuring process, and  $P_{i,j}$  represents the  $j$ th point in scanning line  $i$ . If  $j \geq 2$ , we can build a shape-preserving piecewise bicubic Hermite curve to conjecture the shape and direction of the current scanning line. Suppose  $k$  is a positive integer and let  $1 \leq k < j$  and the coordinates of point  $P_{i,k}$  are  $(x_k, y_k, z_k)$ , then a series of specific Hermite interpolation polynomials can be determined by

$$\begin{cases} H_y(x) = y_k \alpha_k(x) + y_{k+1} \alpha_{k+1}(x) + y'_k \beta_k(x) + y'_{k+1} \beta_{k+1}(x) \\ H_z(x) = z_k \alpha_k(x) + z_{k+1} \alpha_{k+1}(x) + z'_k \beta_k(x) + z'_{k+1} \beta_{k+1}(x) \end{cases}, \quad (7)$$

in which

$$\begin{cases} \alpha_k(x) = (1 + 2 \frac{x-x_k}{x_{k+1}-x_k}) (\frac{x-x_{k+1}}{x_{k+1}-x_{k+1}})^2 \\ \alpha_{k+1}(x) = (1 + 2 \frac{x-x_{k+1}}{x_{k+1}-x_{k+1}}) (\frac{x-x_k}{x_{k+1}-x_k})^2 \\ \beta_k(x) = (x - x_k) (\frac{x-x_{k+1}}{x_{k+1}-x_{k+1}})^2 \\ \beta_{k+1}(x) = (x - x_{k+1}) (\frac{x-x_k}{x_{k+1}-x_k})^2 \end{cases}, \quad (8)$$

and the first derivatives of  $y'_k, y'_{k+1}, z'_k, z'_{k+1}$  in Eq. (7) can be estimated by the following formulas.

When  $1 < k < j$ :

$$\begin{aligned} y'_k &= f'_y(x_k) \\ &= \begin{cases} 0, & \text{if: } \frac{y_{k+1}-y_k}{x_{k+1}-x_k} \cdot \frac{y_k-y_{k-1}}{x_k-x_{k-1}} < 0 \\ \frac{1}{2} \left( \frac{y_{k+1}-y_k}{x_{k+1}-x_k} + \frac{y_k-y_{k-1}}{x_k-x_{k-1}} \right), & \text{if: } \frac{y_{k+1}-y_k}{x_{k+1}-x_k} \cdot \frac{y_k-y_{k-1}}{x_k-x_{k-1}} \geq 0 \end{cases}, \end{aligned} \quad (9)$$

$$\begin{aligned} z'_k &= f'_z(x_k) \\ &= \begin{cases} 0, & \text{if: } \frac{z_{k+1}-z_k}{x_{k+1}-x_k} \cdot \frac{z_k-z_{k-1}}{x_k-x_{k-1}} < 0 \\ \frac{1}{2} \left( \frac{z_{k+1}-z_k}{x_{k+1}-x_k} + \frac{z_k-z_{k-1}}{x_k-x_{k-1}} \right), & \text{if: } \frac{z_{k+1}-z_k}{x_{k+1}-x_k} \cdot \frac{z_k-z_{k-1}}{x_k-x_{k-1}} \geq 0 \end{cases}. \end{aligned} \quad (10)$$

When  $k = 1$ :

$$\begin{aligned} y'_1 &= \begin{cases} 0, & \text{if: } d_y \cdot \frac{y_2-y_1}{x_2-x_1} < 0 \\ 3 \cdot \frac{y_2-y_1}{x_2-x_1}, & \text{if: } |d_y| > 3 \left| \frac{y_2-y_1}{x_2-x_1} \right| \& \frac{(y_2-y_1)(y_3-y_2)}{(x_2-x_1)(x_3-x_2)} < 0 \end{cases}, \end{aligned} \quad (11)$$

$$\begin{aligned} z'_1 &= \begin{cases} 0, & \text{if: } d_z \cdot \frac{z_2-z_1}{x_2-x_1} < 0 \\ 3 \cdot \frac{z_2-z_1}{x_2-x_1}, & \text{if: } |d_z| > 3 \left| \frac{z_2-z_1}{x_2-x_1} \right| \& \frac{(z_2-z_1)(z_3-z_2)}{(x_2-x_1)(x_3-x_2)} < 0 \end{cases}, \end{aligned} \quad (12)$$

where

$$\begin{cases} d_y = \frac{(x_3+x_2-2x_1)(y_2-y_1)}{(x_2-x_1)(x_3-x_1)} - \frac{(x_2-x_1)(y_3-y_2)}{(x_3-x_2)(x_3-x_1)} \\ d_z = \frac{(x_3+x_2-2x_1)(z_2-z_1)}{(x_2-x_1)(x_3-x_1)} - \frac{(x_2-x_1)(z_3-z_2)}{(x_3-x_2)(x_3-x_1)}. \end{cases} \quad (13)$$

When  $k = j$ :

$$\begin{aligned} y'_j &= \begin{cases} 0, & \text{if: } d_y \cdot \frac{y_j-y_{j-1}}{x_j-x_{j-1}} < 0 \\ 3 \cdot \frac{y_j-y_{j-1}}{x_j-x_{j-1}}, & \text{if: } |e_y| > 3 \left| \frac{y_j-y_{j-1}}{x_j-x_{j-1}} \right| \& \frac{(y_j-y_{j-1})(y_{j-1}-y_{j-2})}{(x_j-x_{j-1})(x_{j-1}-x_{j-2})} < 0 \end{cases}, \end{aligned} \quad (14)$$

$$\begin{aligned} z'_j &= \begin{cases} 0, & \text{if: } d_z \cdot \frac{z_j-z_{j-1}}{x_j-x_{j-1}} < 0 \\ 3 \cdot \frac{z_j-z_{j-1}}{x_j-x_{j-1}}, & \text{if: } |e_z| > 3 \left| \frac{z_j-z_{j-1}}{x_j-x_{j-1}} \right| \& \frac{(z_j-z_{j-1})(z_{j-1}-z_{j-2})}{(x_j-x_{j-1})(x_{j-1}-x_{j-2})} < 0 \end{cases}, \end{aligned} \quad (15)$$

where

$$\begin{cases} e_y = \frac{(2x_j-x_{j-1}-x_{j-2})(y_j-y_{j-1})}{(x_j-x_{j-1})(x_j-x_{j-2})} - \frac{(x_j-x_{j-1})(y_{j-1}-y_{j-2})}{(x_{j-1}-x_{j-2})(x_j-x_{j-2})} \\ e_z = \frac{(2x_j-x_{j-1}-x_{j-2})(z_j-z_{j-1})}{(x_j-x_{j-1})(x_j-x_{j-2})} - \frac{(x_j-x_{j-1})(z_{j-1}-z_{j-2})}{(x_{j-1}-x_{j-2})(x_j-x_{j-2})}. \end{cases} \quad (16)$$

According to the above method, the shape-preserving piecewise bicubic Hermite polynomials are created based on reduced point cloud data flow of the current scanning line. Afterwards, Hermite extrapolation is performed to form a conjectured scanning line which is marked in red as shown in Fig. 5, and its analytical formula can be described as:

$$\begin{cases} H_y(x) = y_{j-1}\alpha_{j-1}(x) + y_j\alpha_j(x) + y'_{j-1}\beta_{j-1}(x) + y'_j\beta_j(x), \\ H_z(x) = z_{j-1}\alpha_{j-1}(x) + z_j\alpha_j(x) + z'_{j-1}\beta_{j-1}(x) + z'_j\beta_j(x) \end{cases}, \quad (17)$$

### 2.2.2. Search for the adjacent point set from the previous scanning lines

Based on reduced point cloud data flow from the first stage, the reasoning mechanism first conjectures the curve shape and scanning direction of the current scanning line using Hermite extrapolation as shown in Eq. (17). After that, an estimative point  $P_{est}$  is created to move on the conjectured scanning line with  $P_{i,j}$  as the starting point and the stepping distance of  $\lambda$ . Meanwhile, a bounding sphere is built with point  $P_{est}$  as the center, and the radius of the sphere is set to

$$R_{sph} = \kappa h_{ls} \quad (18)$$

where  $\kappa \in [1, 2]$  is the radius adjustment coefficient and  $h_{ls}$  is the spacing between two adjacent scanning lines. As shown in Fig. 5, the conjectured scanning line with estimative point  $P_{est}$  is used for searching for the adjacent point from the previous scanning line  $i - 1$ . At the very beginning of searching,  $P_{est}$  coincides with  $P_{i,j}$  and the adjacent point of  $P_{est}$  may be found. Suppose  $P_{i-1,u}$  is inside the bounding sphere (i.e.,  $|P_{i-1,u}P_{i,j}| < R_{sph}$ ), then  $P_{i-1,u}$  is the first found adjacent point. As  $P_{est}$  moves along the scanning direction with stepping distance of  $\lambda$ , if  $|P_{est}P_{i-1,u}| < |P_{i,j}P_{i-1,u}|$ , then  $P_{i-1,u}$  is the adjacent point of  $P_{est}$ ; otherwise, discard point  $P_{i-1,u}$  for it is not the adjacent point of  $P_{est}$  but of  $P_{i,j}$ , then point  $P_{est}$  continues to move forward along the scanning direction till the adjacent point of  $P_{est}$  is found; if the adjacent point of  $P_{est}$  cannot be found, stop searching and keep the current sampled point  $P_{i,j+1}$  in the refined point cloud data set as shown in Fig. 4.

If the adjacent point of  $P_{est}$  is found in line  $i - 1$  (e.g.,  $P_{i-1,u+1}$  in Fig. 5), then build a new bounding sphere (with  $P_{i-1,u+1}$  as the center and the radius is  $R_{sph}$ ) to find the adjacent point of it in line  $i - 2$ ; and if the adjacent point cannot be found, stop searching and keep the current sampled point  $P_{i,j+1}$  in the refined point cloud data set as shown in Fig. 4. Next, take the new adjacent point in line  $i - 2$  (e.g.,  $P_{i-2,v+1}$ ) as a new center to build a bounding sphere and repeat the above process until we find three adjacent points in different scanning lines (e.g.,  $P_{i-1,u+1}, P_{i-2,v+1}, P_{i-3,w+1}$  in Fig. 5).

### 2.2.3. Speculation and determination of the coordinates of estimative point

According to adjacent point set  $\{P_{i-1,u+1}, P_{i-2,v+1}, P_{i-3,w+1}\}$ , the coordinates of estimative point can be speculated and determined. As shown in Fig. 5, a bicubic Hermite curve is built using the coordinates of adjacent point set, and it can be expressed as:

$$\begin{cases} H_x(y) = x_{i-2}\alpha_{i-2}(y) + x_{i-1}\alpha_{i-1}(y) + x'_{i-2}\beta_{i-2}(y) + x'_{i-1}\beta_{i-1}(y), \\ H_z(y) = z_{i-2}\alpha_{i-2}(y) + z_{i-1}\alpha_{i-1}(y) + z'_{i-2}\beta_{i-2}(y) + z'_{i-1}\beta_{i-1}(y) \end{cases}, \quad (19)$$

in which  $y$  is an independent variable;  $\alpha_{i-1}(y), \alpha_{i-2}(y), \beta_{i-1}(y), \beta_{i-2}(y)$  is obtained by Formula (8);  $x'_{i-2}, z'_{i-2}$  is acquired by Formulas (9) and (10);  $x'_{i-1}, z'_{i-1}$  is obtained by Formulas (14) to (16). Obviously, the bicubic Hermite curve must be in the curved surface with equation

$$H_x(y) = x_{i-2}\alpha_{i-2}(y) + x_{i-1}\alpha_{i-1}(y) + x'_{i-2}\beta_{i-2}(y) + x'_{i-1}\beta_{i-1}(y) \quad (20)$$

and the conjectured scanning line will pass through this curved surface. Therefore, estimative point  $P_{est}$  can be fixed at the intersection of the conjectured scanning line and the curved surface which is described in Eq. (20). In other words, the coordinates of estimative point  $P_{est}(x_{est}, y_{est}, z_{est})$  can be determined by Eqs. (17) and (20).

### 2.2.4. Verification of estimative point and deletion of sampled point

Estimative point  $P_{est}$  is used to replace  $P_{i,j+1}$  in reduced point cloud data flow of scanning line  $i$ . Immediately afterwards, the new reduced point set which contains point  $P_{est}$  is used for bi-Akima interpolation and there is deviation  $h_{i,k}$  between each original sampled point and interpolated curve. Similarly,  $h_{i,k}$  can be obtained from Eq. (6), where  $i$  is the scanning line number and  $k$  is the serial number of original sampled point  $Q$ . The max deviation  $d_{max}$  of the whole curve can be calculated by the following formula:

$$d_{max} = \max(h_{i,k}), \quad (21)$$

which is then compared with the required accuracy  $\varepsilon$ . If  $d_{max} \leq \varepsilon$ , delete current sampled point  $P_{i,j+1}$  which is input from the reduced point cloud data flow of the first stage. Next, create an estimative flag  $F_{i,j+1} = 1$  to replace point  $P_{i,j+1}$ . This flag takes up only one bit of point cloud data storage space. If  $d_{max} > \varepsilon$ , discard point  $P_{est}$ . After completing the above process, output the refined point cloud data flow which contains the point coordinate and estimative flag information to the data storage devices. As shown in Fig. 4, if  $P_{i,j}$  is not the last point in the last scanning line (i.e.,  $i = i_{max}$  &  $j = j_{max}$ ), and when  $P_{i,j}$  is not the last point in line  $i$  (i.e.,  $j < j_{max}$ ), then let  $j = j + 1$ , build a new shape-preserving piecewise bicubic Hermite curve to conjecture the shape and direction of the current scanning line and create a new estimative point  $P_{est}$  to loop through the above reasoning process (i.e., Section 2.2) until  $P_{i,j}$  is the end point of the current scanning line  $i$  or the data sampling is over.

## 3. Experiment and discussion

In this section, the proposed on-line point cloud data selective sampling method is tested and compared with the other two previous approaches, including the bi-Akima method and the EACDR method. As described in Section 1.1, so far, there are only three on-line point data reduction methods among previous research works (on-line and off-line approaches) that can effectively reduce the amount of point cloud data under the premise of ensuring pre-set accuracy [16,22,23]. The core of the data reduction algorithm described in Ref. [16] is the bi-Akima method; while the essence of data reduction algorithms described in Refs. [22] and [23] is the same, both of which are based on EACDR method. Therefore, we will make a detailed comparison of these three methods: the proposed method, bi-Akima method and the EACDR method. A total of six models with sculptured surface are equidistant sampled with line-by-line scanning path, and initial dense point clouds are hereafter processed by these different methods. Finally, the data processing results are compared and discussed.

**Table 1**

Comparison of reduction performance under different required accuracy in Test A.

Required accuracy (mm)	Number of points			Reduction ratio (%)		
	EACDR method	Bi-Akima method	Proposed method	EACDR method	Bi-Akima method	Proposed method
0.001	34 783	21 720	11 595	88.77	55.43	29.59
0.002	29 260	18 545	9 995	74.68	47.33	25.51
0.005	24 594	15 151	8 223	62.77	38.67	20.99
0.01	22 267	12 444	6 795	56.83	31.76	17.34
0.02	19 866	10 193	5 588	50.70	26.01	14.26
0.05	15 771	8 085	4 441	40.25	20.63	11.33
0.1	11 825	6 996	3 808	30.18	17.86	9.72
0.2	8 622	6 110	3 372	22.01	15.59	8.61
0.5	6 653	5 239	2 867	16.98	13.37	7.32
1	5 924	4 771	2 597	15.12	12.18	6.63



Fig. 6. Typical model of sculptured surface part: wheel hub.

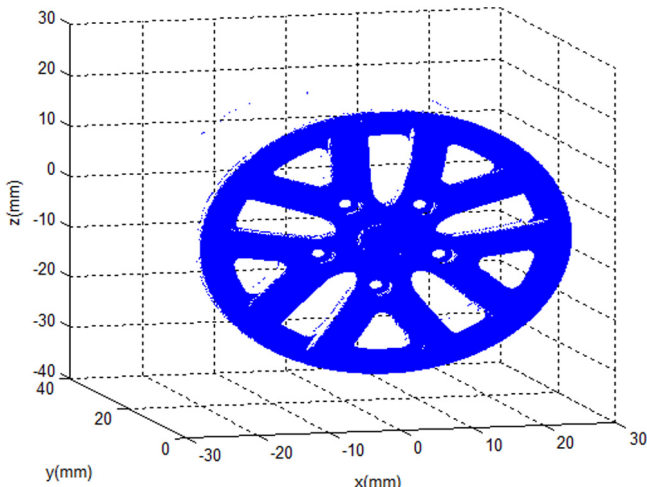


Fig. 7. Spatial distribution of initial point cloud data.

### 3.1. Test A

The sampled model in **Test A** is a wheel hub as shown in Fig. 6. The front of the hub is scanned with line spacing of 0.1 mm, and the distance between adjacent points is 0.05 mm in each scanning line. The initial point cloud data acquisition result is shown in Fig. 7, scanning lines are along X-direction and there are a total of 39 182 sampled points.

Using the same initial point cloud data set as shown in Fig. 7, data reduction comparison is made between different methods under different required accuracies (i.e. from 0.001 mm to 1 mm).

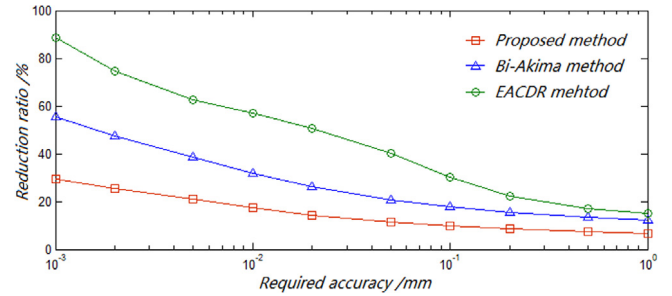
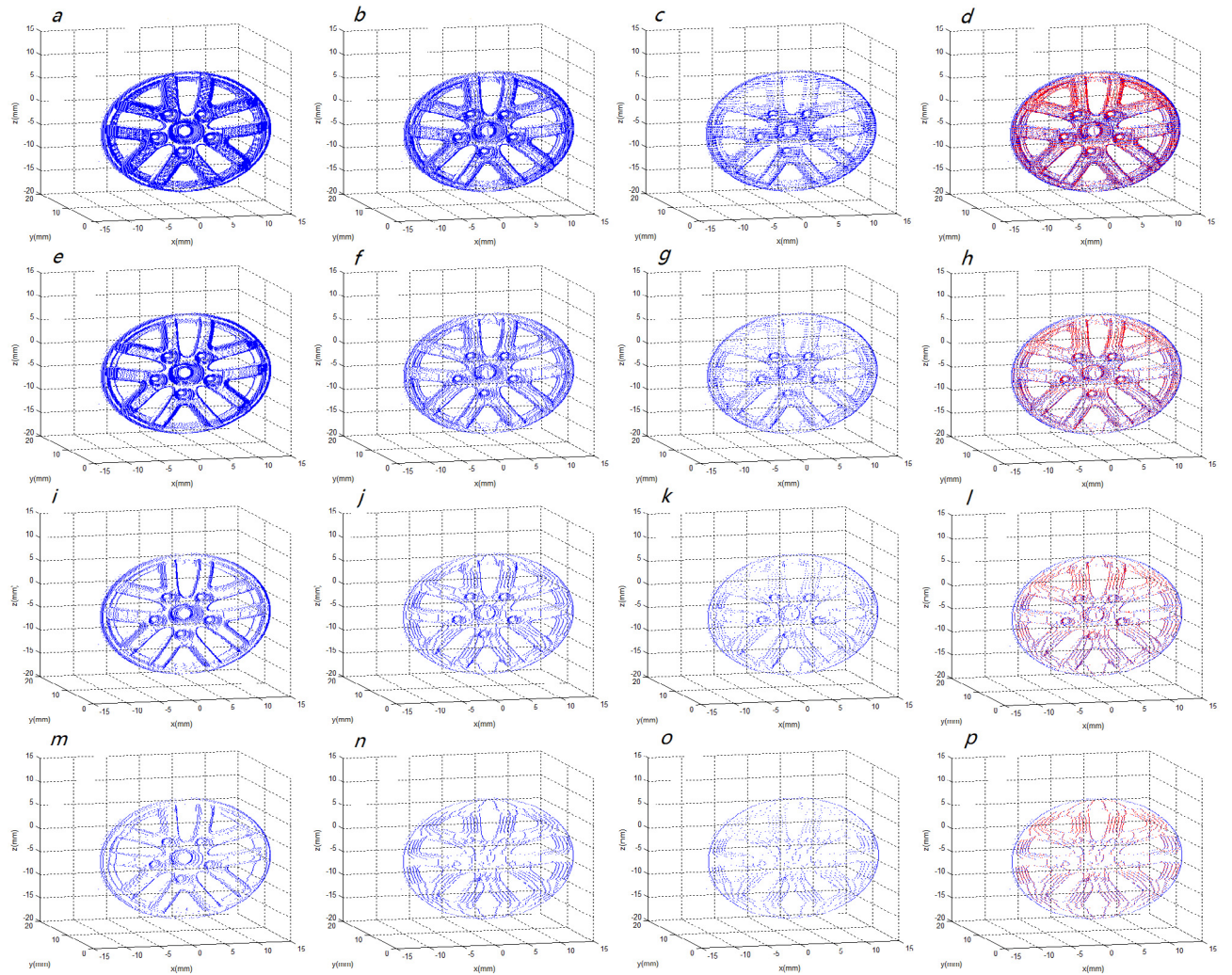


Fig. 8. Comparison of data reduction ratios under different required accuracies.

**Table 1** summarizes the results of data reduction performance including number of points and reduction ratio. Obviously, the proposed method has better data reduction performance than bi-Akima method and EACDR method. The EACDR method gets the largest number of points than the other two methods under the same required accuracy. The number of points obtained by the proposed method is about half of which obtained by bi-Akima method under the same required accuracy.

In order to observe the data reduction performance more intuitively, Fig. 8 provides the comparison of the reduction ratios between these methods under different required accuracies. With the decrease of required accuracy, the reduction ratio increases for all methods; however, for all levels of required accuracies, the proposed reduction method manifests superior reduction ratio than the other two methods.

With the aim to make the comparison more visually, Fig. 9 illustrates the difference between these methods by displaying spatial distributions of reduced point sets under different required accuracies. Subfigures *a*, *e*, *i* and *m* show the point cloud distribution reduced by EACDR method; Subfigures *b*, *f*, *j* and *n* show the point cloud distribution reduced by bi-Akima method; while subfigures *c*, *g*, *k* and *o* give the point cloud distribution refined by the proposed method. By contrast, we can clearly observe the difference of point cloud density between these methods under the same required accuracy. In subfigures *d*, *h*, *l* and *p*, this distinction is further illustrated: the red point sets represent the points deleted by our proposed reasoning mechanism, while the blue ones are the retained points. Take subfigures *m*, *n*, *o* and *p* for example, when using bi-Akima method or EACDR method we can observe that there are many curves roughly along the Z-direction (Fig. 9(m) and (n)), since these two methods can only deal with the point set of the current scanning line which is along the scanning direction (X-axis) and the data redundancy in other directions cannot be well eliminated. With the involvement of our proposed reasoning mechanism, redundant data points are identified and marked in red (Fig. 9(p)), the data redundancy in adjacent scanning layers is eliminated and finally the refined point cloud data is obtained (Fig. 9(o)).



**Fig. 9.** Spatial distributions of point cloud data resampled under different required accuracy  $\varepsilon$ : (a) EACDR,  $\varepsilon = 0.001$  mm; (b) bi-Akima,  $\varepsilon = 0.001$  mm; (c) proposed method,  $\varepsilon = 0.001$  mm; (d) contrast,  $\varepsilon = 0.001$  mm; (e) EACDR,  $\varepsilon = 0.01$  mm; (f) bi-Akima,  $\varepsilon = 0.01$  mm; (g) proposed method,  $\varepsilon = 0.01$  mm; (h) contrast,  $\varepsilon = 0.01$  mm; (i) EACDR,  $\varepsilon = 0.1$  mm; (j) bi-Akima,  $\varepsilon = 0.1$  mm; (k) proposed method,  $\varepsilon = 0.1$  mm; (l) contrast,  $\varepsilon = 0.1$  mm; (m) EACDR,  $\varepsilon = 1$  mm; (n) bi-Akima,  $\varepsilon = 1$  mm; (o) proposed method,  $\varepsilon = 1$  mm; (p) contrast,  $\varepsilon = 1$  mm. (For interpretation of the references to color in this figure legend, the reader is referred to the web version of this article.)

In order to verify the accuracy of the algorithm, Fig. 10 analyzes the spatial distribution of deviation between each initial sampled point and interpolation curve obtained from refined point cloud data under different required accuracies. As can be seen, all the deviations are within the allowable range of required accuracy. Our method can strictly control the deviation within the error tolerance range (i.e., the deviation between each original sampled point and interpolation curve is less than or equal to the required accuracy). In addition, deviations are far less than the required accuracy in most of the measurement area.

### 3.2. Test B

With the purpose to further verify the effectiveness and robustness of the proposed method, a more complex model of sculptured surface part with massive geometric cusps and splicings is tested in this section. The sampled model is a ring with jewels as shown in Fig. 11. It is scanned with line spacing of 0.1 mm, and the distance between adjacent points is 0.05 mm in each scanning line. The spatial distribution of initial point cloud data is shown in Fig. 12, scanning lines are along X-direction and there are a total of 25 263 sampled points.

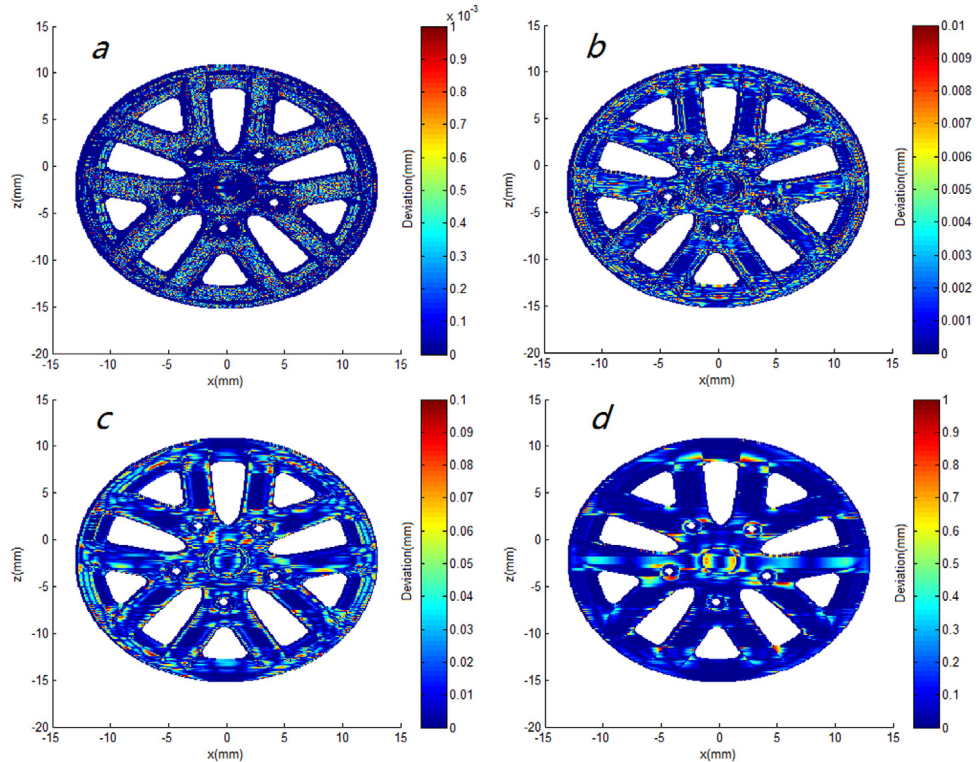
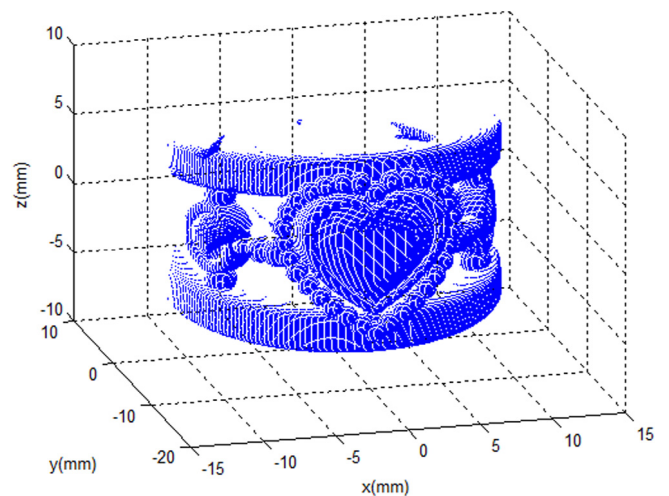
Table 2 summarizes the results of data reduction performance including number of points and reduction ratio. Similar to **Test A**, the proposed method also has the best data reduction performance, and the number of points obtained by the proposed method is about half of which obtained by bi-Akima method under the same required accuracy. The EACDR method gets the largest number of points than the other two methods under the same required accuracy. It is worth mentioning that when the required accuracy is less than 0.005 mm, the data reduction ratio of EACDR method exceeds 90%. Fig. 13 gives the comparison of the reduction ratios between different methods under different required accuracies. With the decrease of required accuracy, the reduction ratio increases for all methods; however, for all levels of required accuracies, the proposed reduction method manifests superior reduction ratio than the other two methods.

Fig. 14 gives spatial distributions of point cloud data resampled under different required accuracies. Subfigures a, e, i and m show the point cloud distribution reduced by EACDR method; Subfigures b, f, j and n show the point cloud distribution reduced by bi-Akima method; while Subfigures c, g, k and o give the point cloud distribution refined by the proposed method. By contrast, we can clearly observe the difference of point cloud density between these methods under the same required accuracy. In

**Table 2**

Comparison of reduction performance under different required accuracy in Test B.

Required accuracy (mm)	Number of points			Reduction ratio (%)		
	EACDR method	Bi-Akima method	Proposed method	EACDR method	Bi-Akima method	Proposed method
0.001	24 475	17 494	8476	96.88	69.25	33.55
0.002	23 462	14 581	7243	92.87	57.72	28.67
0.005	22 527	12 084	6080	89.17	47.83 <sup>a</sup>	24.07
0.01	20 477	10 362	5266	81.06	41.02	20.84
0.02	17 931	8 697	4468	70.98	34.43	17.69
0.05	14 926	6 848	3532	59.08	27.11	13.98
0.1	11 339	5 623	2958	44.88	22.26	11.71
0.2	8 062	4 426	2357	31.91	17.52	9.33
0.5	5 203	3 037	1715	20.60	12.02	6.79
1	3 649	2 265	1288	14.44	8.97	5.10

**Fig. 10.** Spatial distributions of deviation under different required accuracy  $\varepsilon$ : (a)  $\varepsilon = 0.001$  mm; (b)  $\varepsilon = 0.01$  mm; (c)  $\varepsilon = 0.1$  mm; (d)  $\varepsilon = 1$  mm.**Fig. 11.** Typical model of sculptured surface part: ring.**Fig. 12.** Spatial distribution of initial point cloud data.

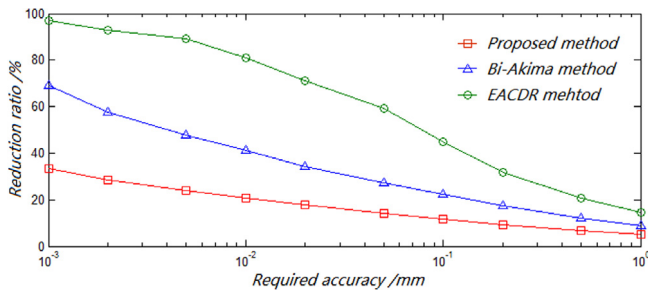


Fig. 13. Comparison of data reduction ratios under different required accuracies.

subfigures *d*, *h*, *l* and *p*, this distinction is further illustrated: the red point sets represent the points deleted by our proposed method, while the blue ones are the retained points. Take subfigures *m*, *n*, *o* and *p* for example, when using bi-Akima method or EACDR method we can observe that there are many curves roughly along the Z-direction (Fig. 14(*m*) and (*n*)), since these two methods can only deal with the point set of the current scanning line which is along the scanning direction (X-axis) and the data

redundancy in other directions cannot be well eliminated. With the involvement of our proposed reasoning mechanism, redundant data points are identified and marked in red (Fig. 14(*p*)), the data redundancy in adjacent scanning layers is eliminated and finally the refined point cloud data is obtained (Fig. 14(*o*))

With the aim to verify the accuracy of the proposed method, Fig. 15 analyzes the spatial distribution of deviation between each initial sampled point and interpolation curve obtained from refined point cloud data under different required accuracies. As can be seen, all the deviations are within the allowable range of required accuracy. Our method can strictly control the deviation within the error tolerance range. In addition, deviations are far less than the required accuracy in most area.

Further, in order to observe the accuracy of the proposed method more visually, Fig. 16 shows surface models reconstructed by different amount of point cloud data, the corresponding number of points  $n_p$  and required accuracy  $\varepsilon$  are marked under each model. With the increasing of the required accuracy, the model surface gradually becomes smoother, and the detail features of the surface increase. When the required accuracy reaches 0.001 mm, the detailed representation of the reconstructed model surface is almost identical to which modeled by the original point

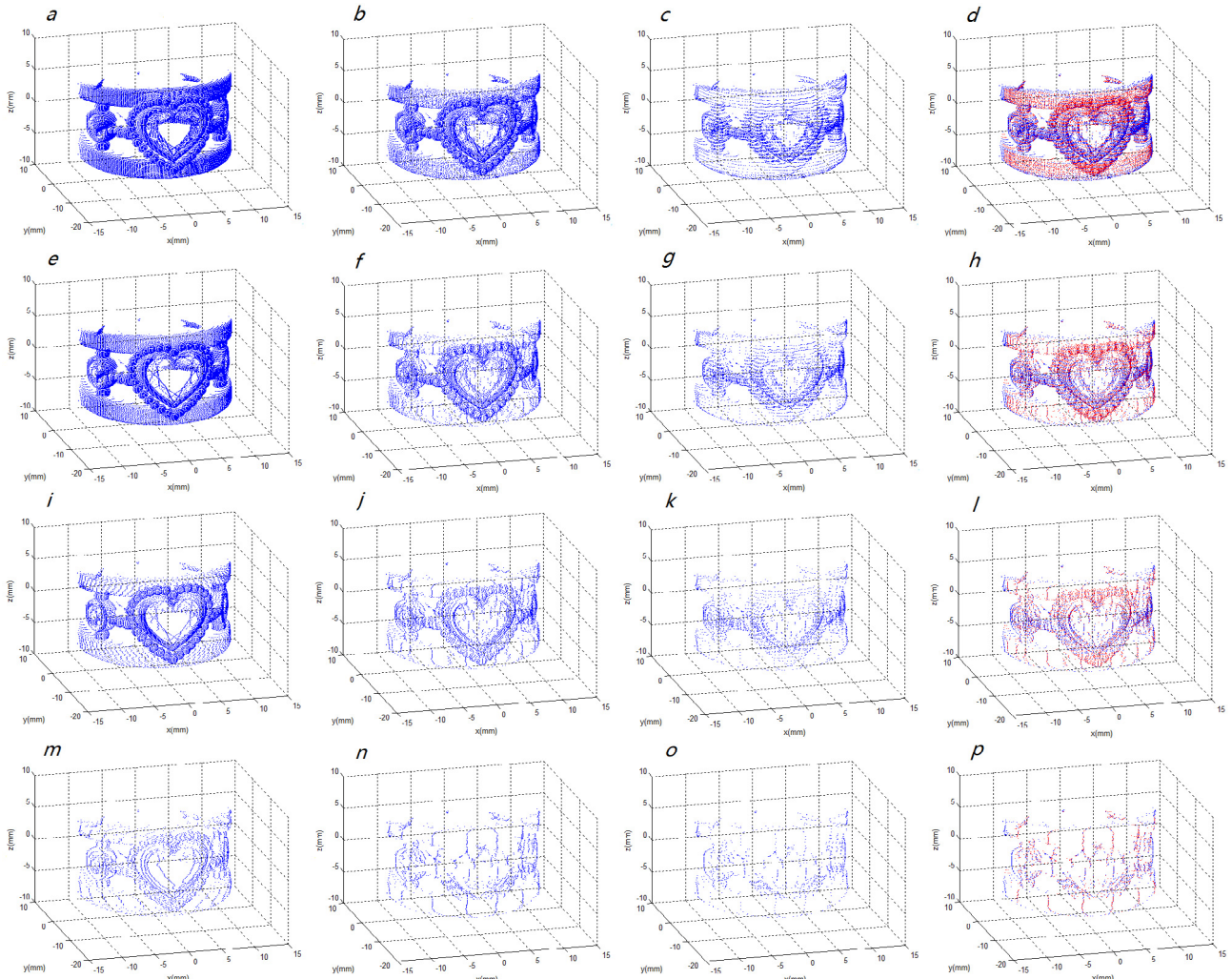
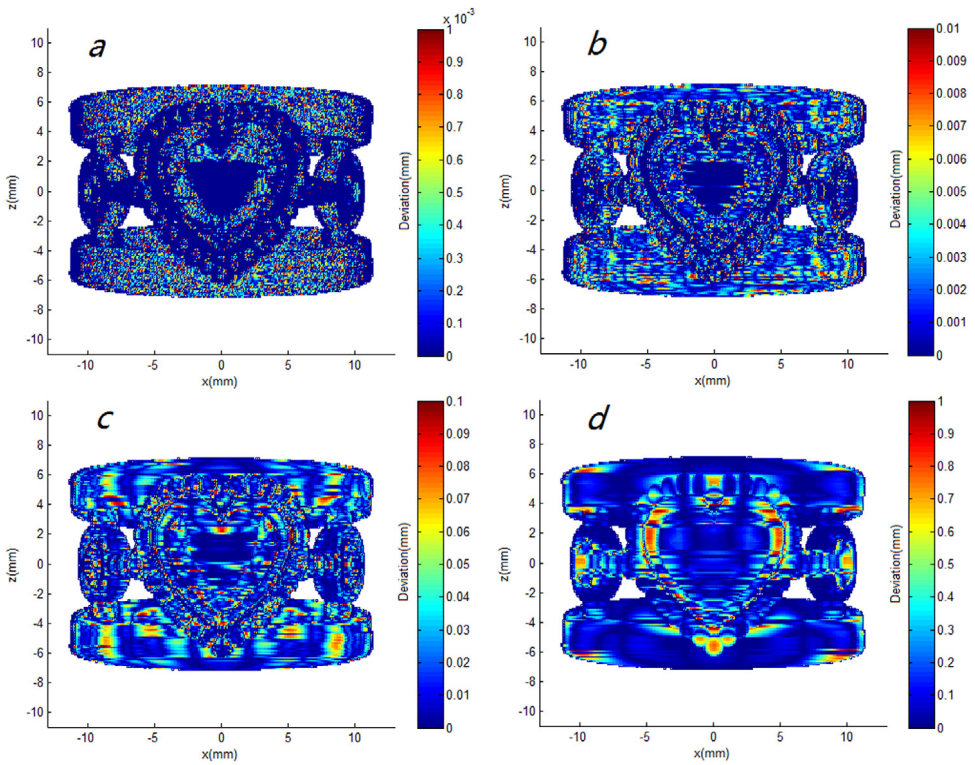
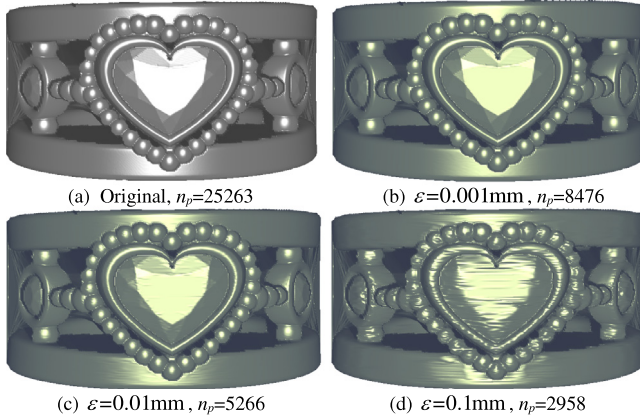


Fig. 14. Spatial distributions of point cloud data resampled under different required accuracy  $\varepsilon$ : (a) EACDR,  $\varepsilon = 0.001$  mm; (b) bi-Akima,  $\varepsilon = 0.001$  mm; (c) proposed method,  $\varepsilon = 0.001$  mm; (d) contrast,  $\varepsilon = 0.001$  mm; (e) EACDR,  $\varepsilon = 0.01$  mm; (f) bi-Akima,  $\varepsilon = 0.01$  mm; (g) proposed method,  $\varepsilon = 0.01$  mm; (h) contrast,  $\varepsilon = 0.01$  mm; (i) EACDR,  $\varepsilon = 0.1$  mm; (j) bi-Akima,  $\varepsilon = 0.1$  mm; (k) proposed method,  $\varepsilon = 0.1$  mm; (l) contrast,  $\varepsilon = 0.1$  mm; (m) EACDR,  $\varepsilon = 1$  mm; (n) bi-Akima,  $\varepsilon = 1$  mm; (o) proposed method,  $\varepsilon = 1$  mm; (p) contrast,  $\varepsilon = 1$  mm. (For interpretation of the references to color in this figure legend, the reader is referred to the web version of this article.)



**Fig. 15.** Spatial distributions of deviation under different required accuracy  $\varepsilon$ : in which: (a)  $\varepsilon = 0.001$  mm; (b)  $\varepsilon = 0.01$  mm; (c)  $\varepsilon = 0.1$  mm; (d)  $\varepsilon = 1$  mm.



**Fig. 16.** Reconstructed models with different number of points ( $n_p$ ) and required accuracies ( $\varepsilon$ ).

cloud, and it is difficult to distinguish the difference between Fig. 16(a) and (b).

### 3.3. Test C

In order to confirm the versatility and adaptability of the proposed method, another four models of sculptured surface parts with various shapes are tested in this section. The sampled models are: impeller, steering wheel, medal and unionsystem as shown in Fig. 17.

In this test, the basic sampling parameters of the sculptured surface models are listed in Table 3. The spatial distribution of initial point cloud data for each model is shown in Fig. 18(a), (e), (i), (m), and the scanning lines are all along X-direction.

Fig. 18 illustrates the difference between different methods by displaying the point cloud data spatial distributions of different

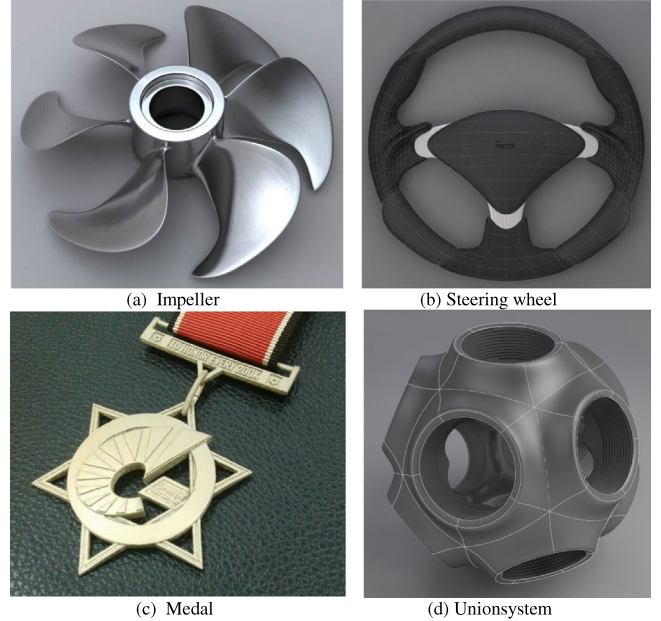


**Fig. 17.** Typical models of sculptured surface parts.

models. Subfigures b, f, j and n show the point cloud distribution reduced by EACDR method; Subfigures c, g, k and o show the point cloud distribution reduced by bi-Akima method; while subfigures d, h, l and p give the point cloud distribution refined by the proposed method. By contrast, we can clearly observe the difference of point cloud density between these methods under the same sampled model and the same required accuracy. The results show that the most sparse point cloud data can be obtained by the proposed method.

**Table 3**  
The sampling parameters of the sculptured surface models in Test C.

Tested models	Line spacing (mm)	Dot spacing (mm)	Number of initial sampled points
Impeller	0.1	0.05	143 149
Steering wheel	0.5	0.5	388 013
Medal	0.1	0.1	171 301
Unionsystem	0.05	0.05	262 437

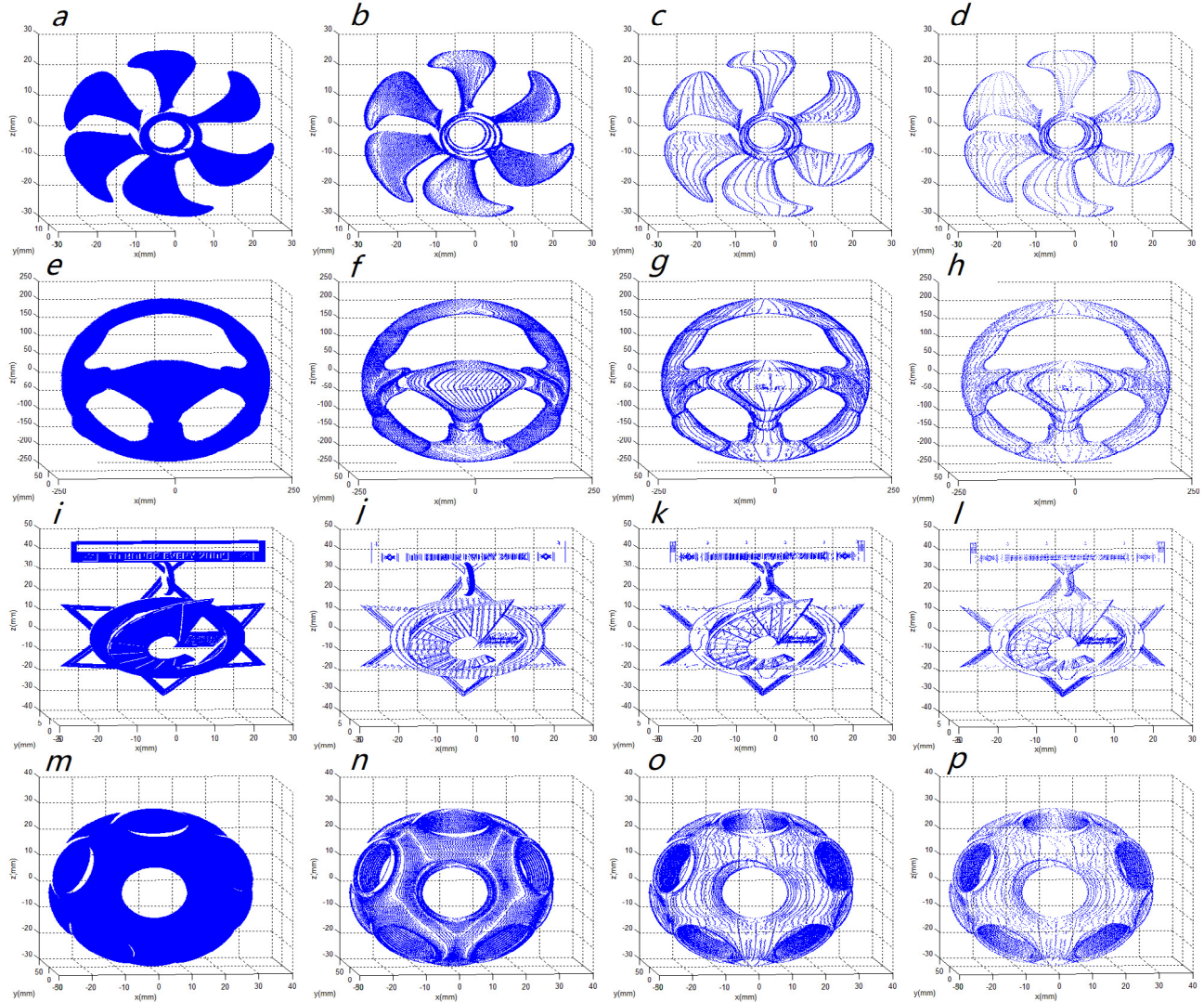


**Fig. 18.** Point cloud data spatial distributions of different models sampled under different required accuracy  $\varepsilon$ : (a) impeller, initial points (b) impeller, EACDR,  $\varepsilon = 0.01$  mm, (c) impeller, bi-Akima,  $\varepsilon = 0.01$  mm, (d) impeller, proposed method,  $\varepsilon = 0.01$  mm, (e) steering wheel, initial points (f) steering wheel, EACDR,  $\varepsilon = 0.05$  mm, (g) steering wheel, bi-Akima,  $\varepsilon = 0.05$  mm, (h) steering wheel, proposed method,  $\varepsilon = 0.05$  mm, (i) medal, initial points (j) medal, EACDR,  $\varepsilon = 0.01$  mm, (k) medal, bi-Akima,  $\varepsilon = 0.01$  mm, (l) medal, proposed method,  $\varepsilon = 0.01$  mm, (m) unionsystem, initial points (n) unionsystem, EACDR,  $\varepsilon = 0.02$  mm, (o) unionsystem, bi-Akima,  $\varepsilon = 0.02$  mm, (p) unionsystem, proposed method,  $\varepsilon = 0.02$  mm.

In order to visually observe the change in data reduction ratio with the required accuracy, Fig. 19 provides the comparison of the reduction ratios between these methods. From the general trend, the reduction ratio increases with the decrease of required accuracy for all methods, and the proposed reduction method manifests superior reduction ratio than the other two methods for all levels of required accuracies. Obviously, the proposed method has better data reduction performance than bi-Akima method and EACDR method, especially when the required accuracy is small (e.g., when required accuracy  $\varepsilon = 0.001$  mm). The number of points obtained by the proposed method is about half of which obtained by bi-Akima method under the same required accuracy. It is worth mentioning that in Fig. 19(c), we

can clearly observe that the data reduction performance of bi-Akima method is worse than that of EACDR method when the accuracy range is between 0.004 mm and 0.4 mm. Except for this medal model, other models (including wheel hub, ring, impeller, steering wheel, unionsystem) in our experiments did not produce this special phenomenon. By analyzing the surface features of these tested models, we found that the medal model does have special characteristics: it is made up of many flat surfaces, while the other models are mainly made up of curved surfaces. This phenomenon indicates that the EACDR method is more suitable for the data reduction of models that are only composed of flat surfaces under certain specific required accuracy. This property is determined by the data reduction principle of the EACDR method.

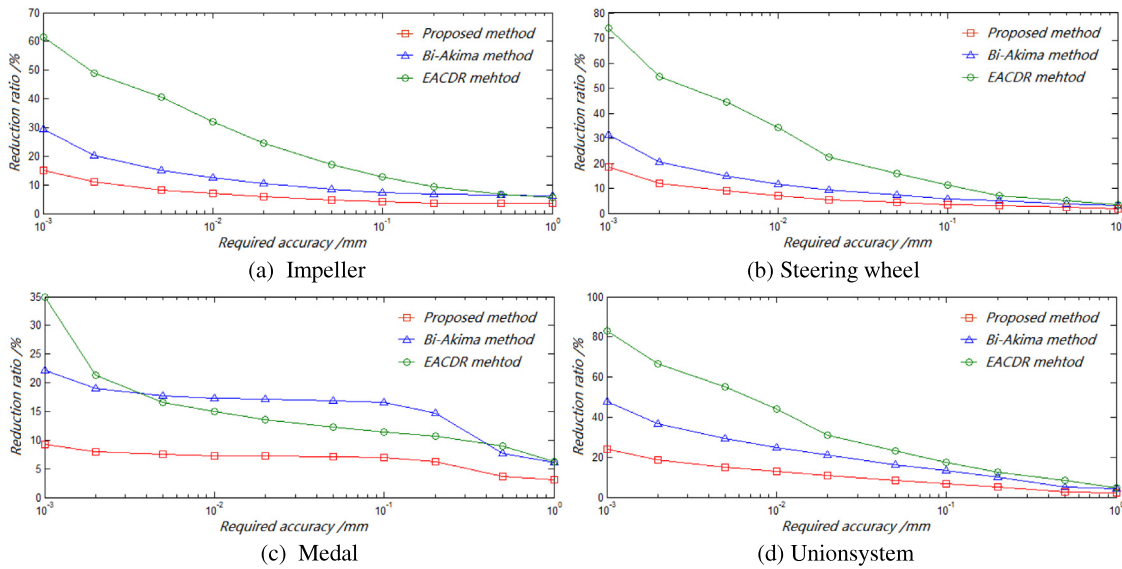


Fig. 19. Comparison of data reduction ratios under different required accuracies.

Experimental result indicates that the proposed on-line point cloud data selective sampling method which involves reasoning mechanism is able to obtain a smaller data reduction ratio than other existing methods under the same required accuracy. The reduction performance of this method is obviously superior to the other on-line point cloud data reduction methods. Moreover, it is capable of strictly controlling the deviation within the error tolerance range, and deviations in most area are far less than the required accuracy. Our proposed method can be utilized in the point cloud data selective sampling process of sculptured surfaces to replace traditional methods.

#### 4. Conclusion

In an attempt to effectively simplify point cloud data from a measured sculptured surface during the on-line point cloud data selective sampling process, this paper presents a novel reasoning mechanism which is capable of eliminating data redundancy caused by spatial similarity of collected point clouds. The reasoning mechanism is based on a predictor-corrector scheme and mainly includes four key aspects: Conjecture, search, speculation and verification. In addition, this mechanism is embedded in our newly designed framework for on-line point cloud data selective sampling of sculptured surface. The new framework mainly consists of two stages. In the first stage, Bi-Akima selective sampling method is employed to reduce the amount of initial point cloud data preliminarily; and in the second stage, the reduced data flow from the first stage is refined based on the reasoning mechanism. The proposed framework is capable of eliminating the redundancy caused by the similarity between adjacent scanning lines and the point cloud data can be effectively simplified. At last, experiment is conducted and shows that the proposed method is capable of obtaining high-quality resampling results with smaller data reduction ratio than other existing on-line point cloud data reduction/selective sampling methods and in particular, it can strictly control the deviation within the error tolerance range (required accuracy  $\varepsilon$ ), which demonstrates the superior performance of the proposed method.

#### Acknowledgments

The research was supported by the National Natural Science Foundation of China (Grant Nos. 51505310, 51435011), the Key

Research and Development Program of Sichuan Province of China (Grant No. 2018GZ0282) and the Science & Technology Ministry Innovation Method Program of China (Grant No. 2017IM040100).

#### References

- [1] Chen L, Jiang ZD, Li B, Ding JJ, Zhang F. Data reduction based on bi-directional point cloud slicing for reverse engineering. *Key Eng Mater* 2010;437:492–6.
- [2] Yan RJ, Wu J, Lee JY, Khan AM, Han CS, Kayacan E, et al. A novel method for 3D reconstruction: Division and merging of overlapping B-spline surfaces. *Comput Aided Des* 2016;81:14–23.
- [3] Pal P, Ballav R. Object shape reconstruction through NURBS surface interpolation. *Int J Prod Res* 2007;45(2):287–307.
- [4] Galetto M, Vezzetti E. Reverse engineering of free-form surfaces: A methodology for threshold definition in selective sampling. *Int J Mach Tool Manuf* 2006;46(10):1079–86.
- [5] Budak I, Hodolic J, Sokovic M. Development of a programme system for data-point pre-processing in Reverse Engineering. *J Mater Process Technol* 2005;162:730–5.
- [6] Li WL, Zhou LP, Yan SJ. A case study of blade inspection based on optical scanning method. *Int J Prod Res* 2015;53(7):2165–78.
- [7] Shi BQ, Liang J, Liu Q. Adaptive simplification of point cloud using k-means clustering. *Comput Aided Des* 2011;43(8):910–22.
- [8] Khameneifar F, Feng HY. Extracting sectional contours from scanned point clouds via adaptive surface projection. *Int J Prod Res* 2017;55(15):4466–80.
- [9] Feng C, Taguchi Y. FasTFit: A fast T-spline fitting algorithm. *Comput Aided Des* 2017;92:11–21.
- [10] Song H, Feng HY. A progressive point cloud simplification algorithm with preserved sharp edge data. *Int J Adv Manuf Technol* 2009;45(5–6):583–92.
- [11] Han H, Han X, Sun F, Huang C. Point cloud simplification with preserved edge based on normal vector. *Optik* 2015;126(19):2157–62.
- [12] Wang YQ, Tao Y, Zhang HJ, Sun S-S. A simple point cloud data reduction method based on Akima spline interpolation for digital copying manufacture. *Int J Adv Manuf Technol* 2013;69(9–12):2149–59.
- [13] Arpaia P, Buzio M, Inglese V. Two-domain real-time algorithm for optimal data reduction: a case study on accelerator magnet measurements. *Meas Sci Technol* 2010;21(3).
- [14] Wang D, He C, Li X, Peng J. Progressive point set surface compression based on planar reflective symmetry analysis. *Comput Aided Des* 2015;58:34–42.
- [15] Xie ZX, Wang JG, Zhang QM. Complete 3D measurement in reverse engineering using a multi-probe system. *Int J Mach Tool Manuf* 2005;45(12–13):1474–86.
- [16] Tao Y, Li Y, Wang YQ, Ma YY. On-line point cloud data extraction algorithm for spatial scanning measurement of irregular surface in copying manufacture. *Int J Adv Manuf Technol* 2016;87(5–8):1891–905.
- [17] Ma X, Cripps RJ. Shape preserving data reduction for 3D surface points. *Comput Aided Des* 2011;43(8):902–9.

- [18] Smith J, Petrova G, Schaefer S. Progressive encoding and compression of surfaces generated from point cloud data. *Comput Graph-UK* 2012;36(5):341–8.
- [19] Morell V, Orts S, Cazorla M, Garcia-Rodriguez J. Geometric 3D point cloud compression. *Pattern Recognit Lett* 2014;50:55–62.
- [20] Chen Z, Zhang T, Cao J, Zhang YJ, Wang C. Point cloud resampling using centroidal Voronoi tessellation methods. *Comput Aided Des* 2018;102:12–21.
- [21] Elkott DF, Veldhuis SC. Isoparametric line sampling for the inspection planning of sculptured surfaces. *Comput Aided Des* 2005;37(2):189–200.
- [22] Wozniak A, Balazinski A, Mayer R. Application of fuzzy knowledge base for corrected measured point determination in coordinate metrology. Annual Meeting of the North American Fuzzy Information Processing Society; 2007, p. 135–9.
- [23] Jia ZY, Lu XH, Wang W, Yang JY. Data sampling and processing for contact free-form surface scan-tracking measurement. *Int J Adv Manuf Technol* 2010;46(1–4):237–51.
- [24] Wang Y, Yang D, Liu Y. A real-time look-ahead interpolation algorithm based on Akima curve fitting. *Int J Mach Tool Manuf* 2014;85:122–30.